段差を有する外ダイアフラム形式コンクリート充填角形鋼管柱梁接合部パネルに関する実験的研究

牟, 犇
九州大学大学院人間環境学府空間システム専攻 : 博士後期課程

松尾, 真太朗
九州大学人間環境学研究院都市・建築部門

池田, 竜輔
九州大学大学院人間環境学府空間システム専攻 : 修士課程

河野, 昭彦
九州大学人間環境学研究院都市・建築学部門

https://doi.org/10.15017/1515830

出版情報：都市・建築学研究. 26, pp.101-110, 2014-07-15. Faculty of Human-Environment Studies, Kyushu University
バージョン：
権利関係：

都市・建築学研究　九州大学大学院人間環境学研究院紀要　第26号，2014年7月
J. of Architecture and Urban Design, Kyushu University, No.26, pp.101～110, July. 2014

段差を有する外ダイアフラム形式コンクリート充填角形鋼管柱梁接合部パネルに関する実験的研究

An Experimental Study on Offset H-shaped Steel Beams to Square Concrete Filled Steel Tubular Column Connection Panels with Exterior Diaphragms

牟　犇*，松尾真太朗**，池田竜輔***，河野昭彦**
Ben MOU*, Shintaro MATSUO**, Ryusuke IKEDA*** and Akihiko KAWANO**

The purpose of this paper is to investigate monotonic and cyclic behavior of offset H-shaped steel beams to square concrete filled steel tubular (CFT) column connection panels with exterior diaphragms. The main objective of this research is to establish the plastic strength calculation method for the panels based on the limit analysis. Four cruciform subassemblages are tested under the cyclic and monotonic loading in order to obtain fundamental data for the collapse mechanism of the panels. The plastic strength calculation method is proposed and the accuracy of the method is demonstrated in comparison with the experimental results. Major findings are as follows: 1) the assumed collapse mechanisms coincide with the experimental results, 2) the proposed formulae underestimate the experimental strength of the connection panels.

Keywords: *Offset beam-to-column connection panel, Exterior diaphragm, Concrete filled steel tube, Collapse mechanism, Plastic strength*
段違いパネル、外ダイアフラム、コンクリート充填鋼管、崩壊機構、全塑性耐力

1. Introduction

Steel-concrete composite structures have been gradually adopted in high-rise buildings because these structural systems combine the advantage of high capacity of the concrete with favorable ductility of the steel. Modern composite structures not only meet the needs of structural performance but also satisfy the demands of lower weight. Offset H-shaped steel beam to square CFT column connections with exterior diaphragms, as illustrated in Fig.1, have been applied in recent years.

For the researches on the exterior diaphragm type connection, several experiments have been conducted and the empirical formulae predicting the local strength of the connections have been proposed[1),2)]. Furthermore divided exterior diaphragms were developed to improve the workability[3),4)]. As for the researches on the offset beam-to-column connection, Kuwahara et al.[5)] and Matsuo et al.[6)] experimentally and analytically proposed the strength of connection panels with through diaphragm and exterior diaphragm, respectively. However, offset H-shaped steel beams to square CFT column connections have not been prevalent due to a lack of provisions for this type connections. When the structure designers want to make adjacent beam's depth different, they, for example, often adopt the vertical haunch construction method for beam end connections in the current design. However, since it takes much trouble to fabricate the vertical haunch, more simple connection type is desired. The offset beam to CFT column connection with exterior diaphragms is a construction method that can respond well to this request. Thus, it is necessary to examine behavior of the offset beam to CFT column connection panel.

Extensive researches on the beam to CFT column connections have been done. Researches by Matsui[7)], Yokoyama[8)] and Kawano et al.[9)] on welded beam to CFT column connections with interior and exterior diaphragms, respectively, indicated that CFT connection panel developed a complex stress state and was susceptible to local buckling and fracture. Cyclic tests on CFT moment connections were conducted by Kanatani et al. [10)], as well as Kawano et al. [11)], in which shear yielding of the steel tube within the connection panel zone occurred. Their test results demonstrated that ductile hysteretic behavior of the specimens can be achieved for a large shear deformation.

*　空間システム専攻　博士後期課程
**　都市・建築学部門
***　空間システム専攻　修士課程

Researches on the shear strength of panel zone of steel beam to CFT column moment connections have been nearly developed. The AIJ standards contain provisions for the allowable and ultimate strengths of the panel zone under lateral seismic loading. The formula is obtained by superposing the shear strength of steel and concrete directly[12]. Based on a series of experimental results, Koester[13] proposed a formula for the panel zone, which is derived from regression analysis. Cheng and Chung conducted a series of experiments on the beam to CFT column connection and proposed a stress-strain model to simulate the shear force of panel zone[14),15]. Considering the confinement provided by the steel tubular flange, a new theoretical compression strut mechanism was proposed by Fukumoto[16),17)], which is based on a tri-linear shear deformation model for the steel tube and ultimate capacity assessment for the concrete.

It is expected that the behavior of the composite connection composed of offset H-shaped steel beams and CFT column is similar to that of the joints with the same depth beams. But the load transferring mechanisms and the collapse mechanisms of the composite connections will be different due to the differences in beam depth, and the applicability of the joint details for the beam-to-column connection with exterior diaphragms should be assessed as well. However, it seems that there are limited data on the performance of this composite connections in previous studies. This paper is thus to investigate the seismic performance of the offset H-shaped steel beam to square CFT column connection panels with exterior diaphragms. The main objectives of the research are as follows: (1) to investigate the influence of difference in beam depth on the connection performance; (2) to propose the collapse mechanisms for both steel and concrete panels; (3) to evaluate the resistance of the connection panels by the plastic strength of the panel based on the limit analysis.

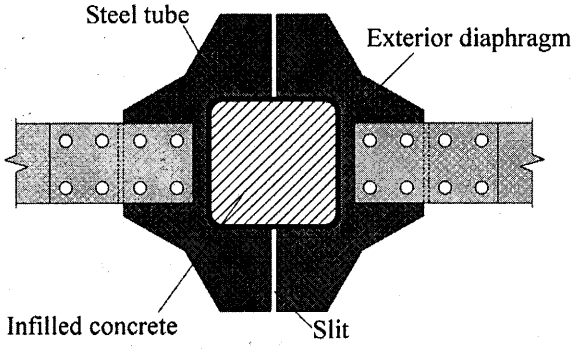

(a) Divided exterior diaphragm

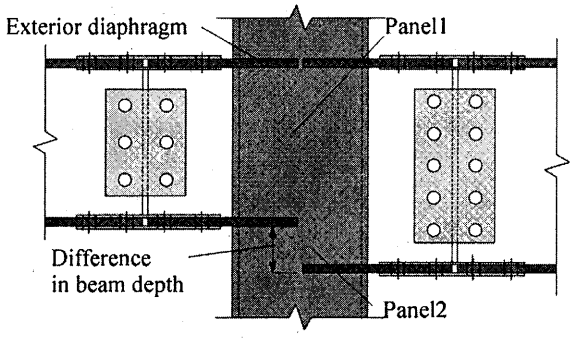

(b) Offset beam to column connection

Fig.1 Offset H-shaped steel beam to square CFT column connection with exterior diaphragms

2. Experimental Investigation

2.1 Subassemblages and test program

Summaries of specimens are listed in Table1. Four specimens are selected to investigate the behavior of the offset H shaped steel beam to CFT column connection panel. The typical specimen and details of exterior diaphragms are shown in Figs.2 and 3, respectively. The main experimental variables are differences in beam depth (Δd_b=0mm, 75mm, 150mm) and loading types (cyclic loading and monotonic loading). For the column, a hollow steel tubular section of 200×200×9 mm is manufactured by BCR295, which is specified in the standards authorized by the minister of land, infrastructure, and transport in Japan. Built-up beams are applied for beam1, which have flange plates of 120×12mm and web plate of 300×6mm. Beam2 is identical to beam1 except the beam depth ranging from 150mm to 300mm. Exterior diaphragms and beams are made by SN490B, which is specified in the Japanese industrial standards. Exterior diaphragms are the same thickness as the beam flange and welded with beam flanges and around the steel tube.

The material properties are listed in Table2. The yield strength is obtained from the value of lower yield point σ_y. And the Young's modulus is measured by the secant stiffness

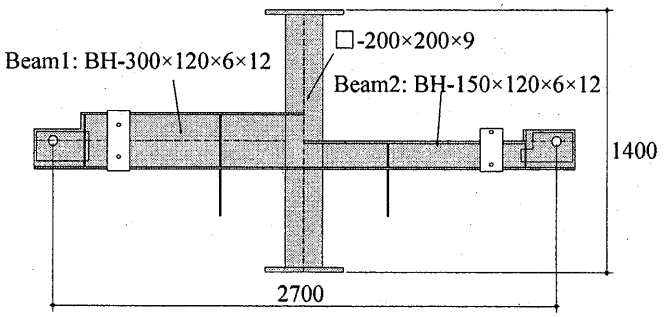

Fig.2 Specimen (No.3 and No.4)

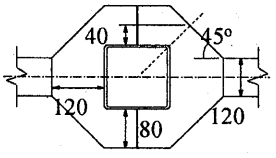

Fig.3 Details of exterior diaphragm

Table1 Details of specimens

No.	Steel column (BCR295)	Beam1 (SN490B)	Beam2 (SN490B)	Δd_b (mm)	Compressive strength (N/mm²)	Loading type
1	□-200×200×9	BH-300×120×6×12	BH-300×120×6×12	0	36.0	Cyclic
2			BH-225×120×6×12	75	36.5	
3			BH-150×120×6×12	150	37.9	
4					36.8	Monotonic

* BCR295 is the material approved by the ministry of land, infrastructure, and transport in Japan.
* SN490B is the material specified in Japanese industrial standard.

Table2 Material properties of steel

Part	Steel type	Thickness (mm)	Young's modulus (N/mm²)	Yield stress (N/mm²)	Tensile stress (N/mm²)	Elongation (%)
Beam web	SN490B	6.2	201,700	399	531	21
Beam flange Exterior diaphragm	SN490B	11.9	207,240	351	503	25
Square column	BCR295	9.0	192,300	371	432	33

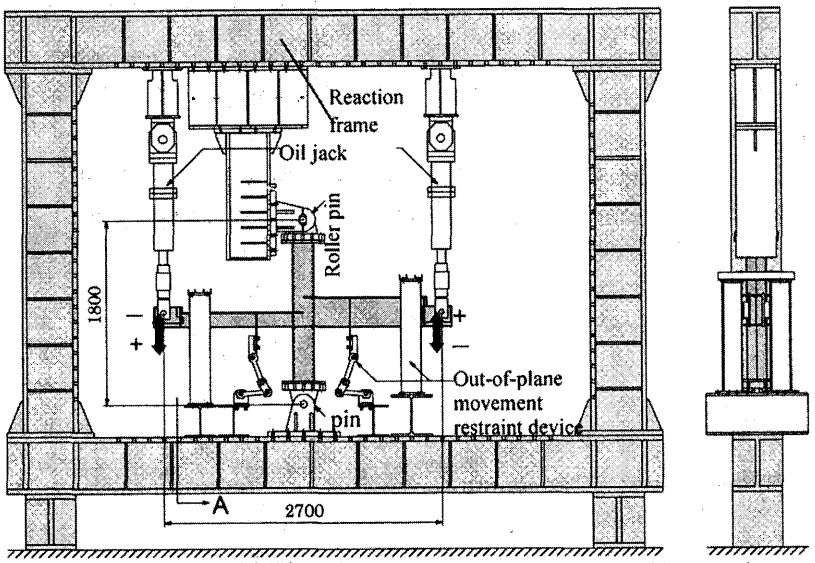

(a) Elevation (b) A section

Fig.4 Overall view of test setup

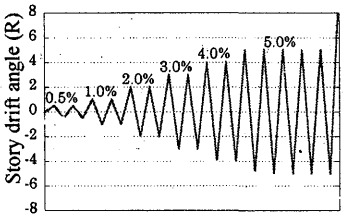

Fig.5 Loading history

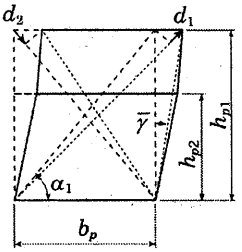

Fig.6 The measuring method of panel zone

between the 1/3 σ_y point and 2/3 σ_y point. Normal concrete is applied for the specimens. It is poured in the hollow steel tubular column with vibration, and then the specimens are placed upright until the test. The compressive strength of the concrete is determined by standard cylinder compression tests.

2.2 Testing procedure

The general arrangement of the test setup and the loading directions are illustrated in Fig.4. A pin and vertically-roller support connected with a steel frame at the top of the square CFT column. And a pin support is at the end of column bottom. The length between pin and pin roller is 1800mm, and the length between the two loading points is 2700mm. Two hydraulic jacks of 500kN capacity are used to apply the loadings to the beam ends in the vertical direction. In the positive direction, the beam1 end is pulled upward, while the beam2 end is pushed downward. In the negative direction, the loadings on the beam ends are reversed. Out-of-plane movement restraint devices are specially designed to prevent the unexpected instability and lateral torsional buckling of the specimens, as shown in Fig.4.

The vertical loading applied on the right and left sides of the specimen are controlled with the opposite of the direction in order to simulate the story drift angle caused by lateral loading. The loading program used for displacement control is shown in Fig.5. The story drift angle (R) is defined as the ratio of the vertical displacement between the ends of beam to the distance between the pins. The test history begins with two cycles repeat for story drift angle amplitudes of ±0.005, ±0.01, ±0.02, ± 0.03, and ±0.04 rad, subsequently, 5 cycles of ±0.05 rad is applied, and ultimately, the magnitude of the story drift angle increases gradually in the positive loading direction until R is approximately equal to 0.08 rad. For the

test under monotonic loading, the magnitude of the story drift angle increases gradually in the negative loading direction until R is approximately equal to -0.074 rad.

2.3 Measurements

The shear force of beams is measured by the load cells on the oil jacks. The vertical displacement in the end of the beam, the horizontal and vertical displacement of beam-to-column connection and pins are measured by the displacement transducers. The measuring method of panel zone is shown in Fig.6. The shear deformation angle of panel zone (γ) is obtained by Eq. (1).

$$\gamma = \frac{d_1 + d_2}{2h_{p1}\cos\alpha} \tag{1}$$

where, h_{p1} : the measured height of the entire panel; h_{p2} : the measured height of the panel1; b_p : the measured width of the entire panel.

The shear force of the panel1 ($_{p1}Q$), panel2 ($_{p2}Q$) and entire panel ($_{p}Q$) are obtained by Eqs. (2), (3) and (4a), respectively.

$$_{p1}Q = \left(\frac{_{b1}Q}{d_{b1}} + \frac{_{b2}Q}{d_{b2}}\right)\frac{L_b - d_c}{d_{b1}} - \frac{_{b1}Q + {}_{b2}Q}{2}\frac{L_b}{L_c} \tag{2}$$

$$_{p2}Q = \frac{_{b1}Q}{d_{b1}}\frac{L_b - d_c}{2} - \frac{_{b1}Q + {}_{b2}Q}{2}\frac{L_b}{L_c} \tag{3}$$

$$_{p}Q = \left(\frac{L_b - d_c}{d_{b1}} - \frac{L_b}{L_c}\right)\frac{_{b1}Q + {}_{b2}Q}{2} \tag{4a}$$

$$_{p}Q = {}_{p2}Q + (_{p1}Q - {}_{p2}Q)\frac{d_{b2}}{d_{b1}} \tag{4b}$$

where, d_c : the distance between the centers of thickness of two panel flanges ; d_{b1} : the distance between the centers of thickness of two beam1 flanges ; d_{b2} : the distance between the centers of thickness of two beam2 flanges ; L_b : the distance between the two loading points ; L_c : the distance between the pins in the column; $_{b1}Q$: the shear force of beam1; $_{b2}Q$: the shear force of beam2.

2.4 Discussion of the test results

There are many common aspects among the specimens. No.1 to No.3 were applied to the cyclic loadings. The three specimens responded linearly during small rotation cycles. The shear strength of entire panel did not increase significantly after exceeding the linear limit. All the specimens behaved in a ductile manner throughout the test and no signs of fracturing were observed. The failures of the test specimens are related with the differences in beam depth and different loading directions.

Cyclic and monotonic behavior of the entire panel zone is generally evaluated through the hysteretic loops and monotonic curve of shear force versus shear deformation

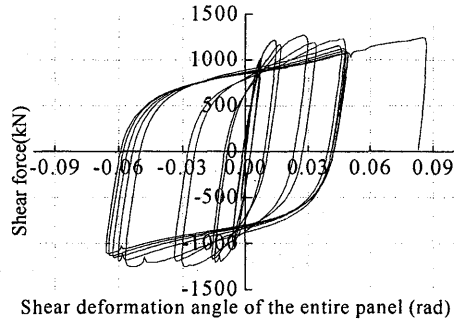

(a) No.1 (Δd_b=0, cyclic loading)

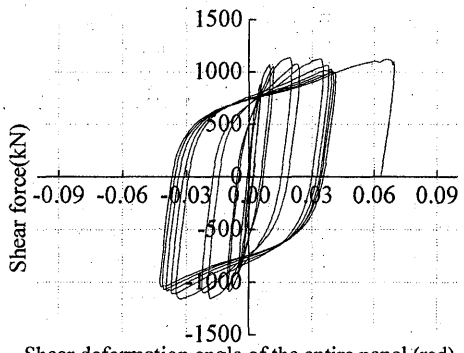

(b) No.2 (Δd_b=75, cyclic loading)

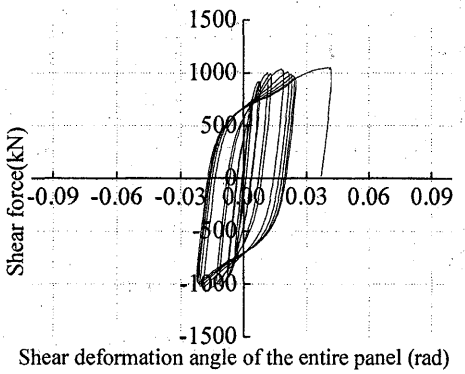

(c) No.3 (Δd_b=150, cyclic loading)

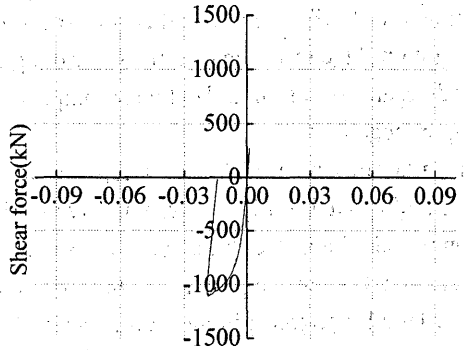

(d) No.4 (Δd_b=150, monotonic loading)

Fig.7 The relationship between shear force and shear deformation angle of the entire panel

angle of the entire panel, as illustrated in Fig.7. The hysteretic loops of No.1 to No.3 are stable. While the differences in beam depth increase, the maximum shear deformation of entire panel zone decreases gradually. The maximum shear force and shear deformation of No.4 have little differences with these of No.3 under the negative loadings. It indicates that the loading type has little influence on the shear force and shear deformation of entire panel zone. The maximum shear strengths and shear deformation angle of entire panel zone are summarized in Table3.

Table3 Experimental shear force of entire panel

No.	Δd_b [mm]	Positive loading		Negative loading	
		pQ_{max} [kN]	$p\gamma_{max}$ [rad]	pQ_{max} [kN]	$p\gamma_{max}$ [rad]
1	0	1,269	0.028	1,251	0.029
2	75	1,141	0.019	1,162	0.033
3	150	1,050	0.040	1,063	0.018
4	150	-	-	1,109	0.019

The shear deformations of panel1 and panel2 are compared by skeleton curve as shown in Fig.8. The skeleton curves are based on the proposal by Akiyama and Kato[18]. The method is shown in Fig.9. Point A is the peak point in the first cycle. Point B is the point of shear force equals to A in the second cycle. Point C is the peak point in the second cycle. Under the positive loading, the skeleton curve contains the curve of 0A in the first cycle, and then the curve of BC is offset to make the point A to coincide with point B. This new curve of AC` is the skeleton curve in the second cycle. The above procedures are repeated for the remaining cycles. Finally, the skeleton curve can be obtained. The shear strain of panel1 and panel2 are calculated by the tests of rosette gauges in the middle of panel1 and panel2, respectively. It is found that the shear deformation of connection panel concentrates on panel1, whether the specimens are under cyclic loading or under monotonic loading. And the deformation of panel2 is very limited. The observed failure phenomena of the connection panel zone under the cyclic and monotonic loading are shown in Fig.10. For No.1, excessive shear deformation of entire panel is found. While, as for No.2 to No.4, it is noting that panel1 occurs large shear deformation. Owing to the differences in beam depth, visible outward deformation is observed on the column flange connected with the exterior diaphragms.

The failures of infilled concrete at the panel are obtained by removing part of the skin plate of the tube around the connection. Fig.11 shows photographs of the exposed concrete in all specimens. Several diagonal cracks are observed on the surface of concrete. The formations of the diagonal cracks indicate that the infilled concrete forms arch mechanisms bearing shear force transmitted by the diaphragms. The lo[illegible]oncrete is easily removed from the panel zone by a handheld chipping hammer. Obvious asymmetries cross diagonal cracks are found in No.2. The

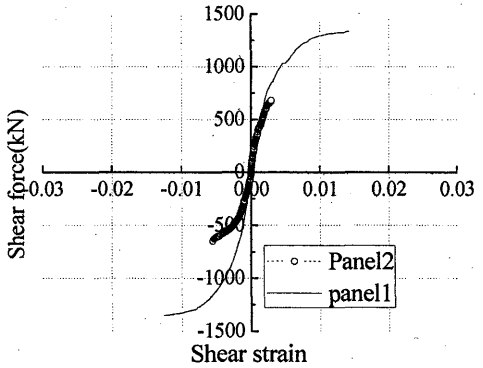

(a) No.2 (Δd_b=75, cyclic loading)

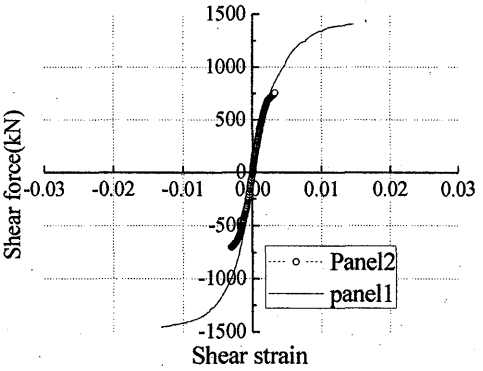

(b) No.3 (Δd_b=150, cyclic loading)

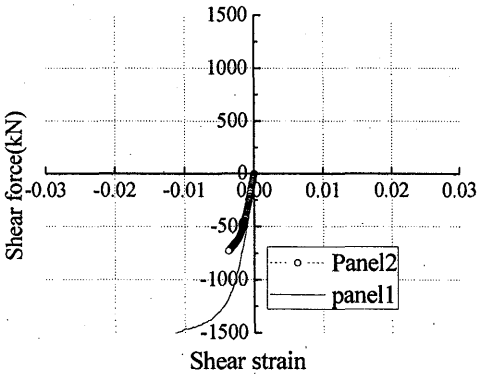

(c) No.4 (Δd_b=150, monotonic loading)

Fig.8 Comparisons of shear strain of panel1 and panel2

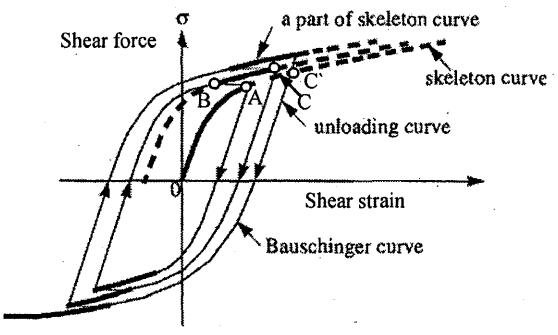

Fig.9 Rule of skeleton curve

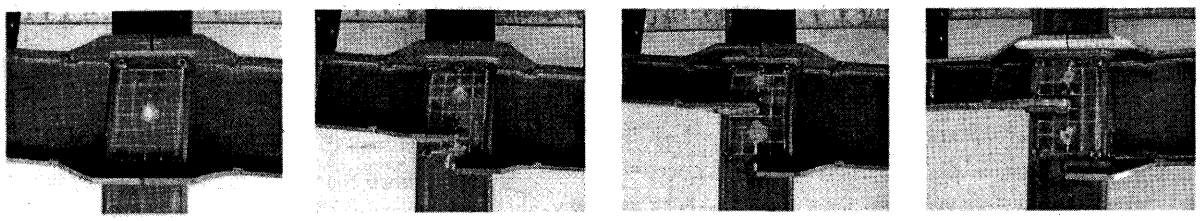

(a) No.1 (Δd_b=0) (b) No.2 (Δd_b=75) (c) No.3 (Δd_b=150) (d) No.4 (Δd_b=150)

Fig.10 Residual deformation of connection panel zone

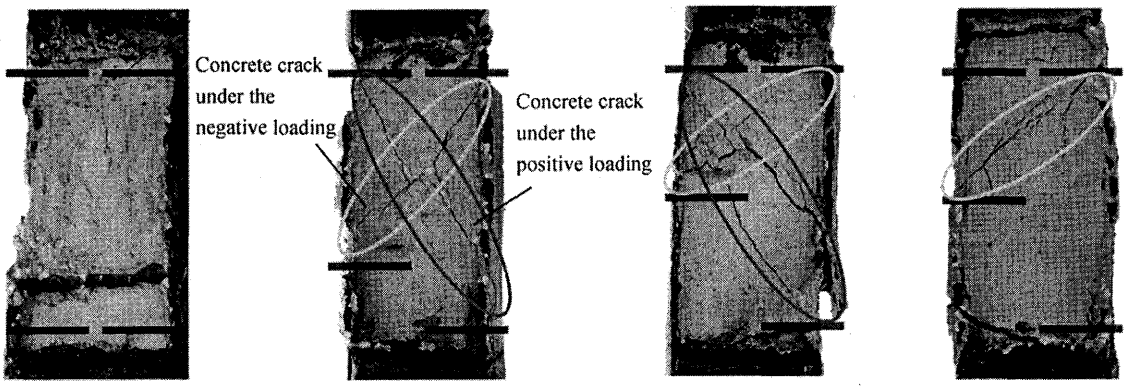

(a) No.1 (cyclic loading) (b) No.2 (cyclic loading) (c) No.3 (cyclic loading) (d) No.4 (monotonic loading)

Fig.11 Typical failure modes of core concrete under monotonic and cyclic loading

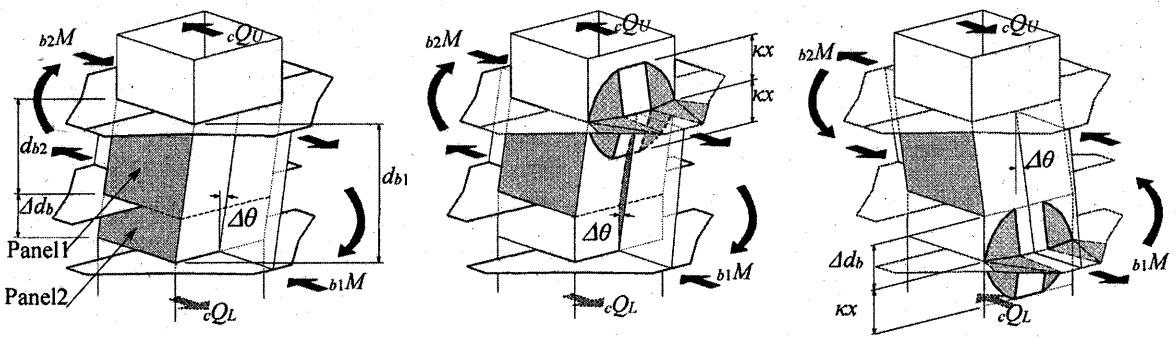

(a) Collapse mechanism of steel for mechanism E (b) Collapse mechanism of steel for mechanism P_A (c) Collapse mechanism of steel for mechanism P_B

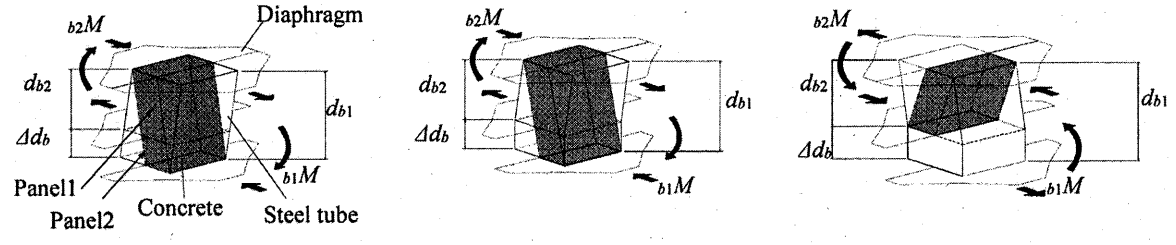

(d) Collapse mechanism of concrete for mechanism E (e) Collapse mechanism of concrete for mechanism P_A (f) Collapse mechanism of concrete for mechanism P_B

Fig.12 Assumed collapse mechanism

formations of the diagonal cracks indicate that the infilled concrete follows arch mechanism under the cyclic loading. Owing to the specimens under the positive loading, the entire concrete panel zone is in the compression condition and all the concrete participates in resisting connection shear. While, due to the specimens under the negative loading, only the panel1 is in the compression condition. The concrete of panel2 has no contributions to resist shear force. Therefore,

the concrete panel zone forms different height compression arches in the different direction loadings. The behavior of concrete panel zone in No.3 is similar to that in No.2. Owing to the difference in beam depth, the height of the diagonal cracks in the negative loading in No.3 is smaller than that in No.2. As for No.4, one diagonal crack is observed in panel1, while the concrete of panel2 is intact. These indicate that only concrete of panel1 bear shear force transmitted by the diaphragms in the negative loading. Meanwhile, concrete of panel2 has no contributions to the panel strength.

3. Collapse mechanisms and plastic strength

3.1 Collapse mechanism

The collapse mechanisms of the offset H-shaped steel beam to square CFT column connection panel with exterior diaphragms are assumed as shown in Fig.12. As for Fig.12 (a), both steel panel1 and panel2 deform plastically. And the concrete of panel1 and panel2 form arch mechanism. That is referred to as entire collapse mechanism (hereinafter mechanism E). When connections are applied to the positive loadings as shown in Fig.12 (b), the plastic deformation emerges on panel1, out-of-plane deformation arises in the column flange connected with the exterior diaphragms and beam1 web yield. The concrete of panel1 and panel2 form arch mechanism. That is referred to as mechanism P_A. When connections are applied to the negative loadings as shown in Fig.12 (c), the plastic deformation emerges on the panel1, out-of-plane deformation arise in the column flange connected with the lower exterior diaphragms, and only concrete of panel1 forms arch mechanism. That is referred to as mechanism P_B.

3.2 Formulae of the plastic strength

For the mechanisms E, P_A and P_B, the internal virtual works of steel tube (${}_sW_p^E$, ${}_sW_p^{P_A}$ and ${}_sW_p^{P_B}$) are given by Eqs.(5)[5] and (6), respectively.

$$ {}_sW_p^E = 2td_cd_{b1}\frac{\sigma_{cy}}{\sqrt{3}}\Delta\theta \tag{5} $$

$$ {}_sW_p^{P_A} = {}_sW_p^{P_B} = 2td_cd_{b2}\frac{\sigma_{cy}}{\sqrt{3}}\Delta\theta \tag{6} $$

where, d_c=D-t, D : column width, t : column thickness, d_{b1}=D_{b1}-t_{bf1}, D_{b1} : beam1 depth, t_{bf1} : beam1 flange thickness, σ_{cy} : yield stress of column tube, d_{b2}=D_{b2}-t_{bf2}, t_{bf2} : beam2 flange thickness, D_{b2} : beam2 depth and $\Delta\theta$: virtual rotation angle.

For the mechanisms P_A and P_B, the collapse mechanism of exterior diaphragm is shown in Fig.13. The internal virtual work of exterior diaphragm (W_d) is given by Eq. (7)[4].

$$ W_d = \frac{\sqrt{3}}{3}t_d\cdot\sigma_{dy}\sqrt{4(x+t/2-b)^2+a^2}\cdot\delta + \frac{2(1+\tan\theta)}{\sqrt{3(1+4\tan^2\theta)}}\cdot h_d t_d\sigma_{dy}\delta \tag{7} $$

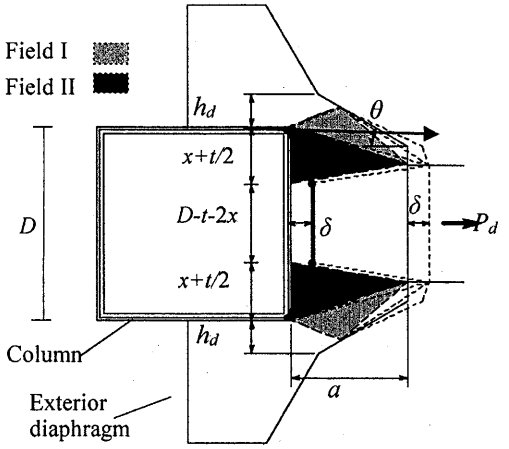

Fig.13 Collapse mechanism of exterior diaphragm

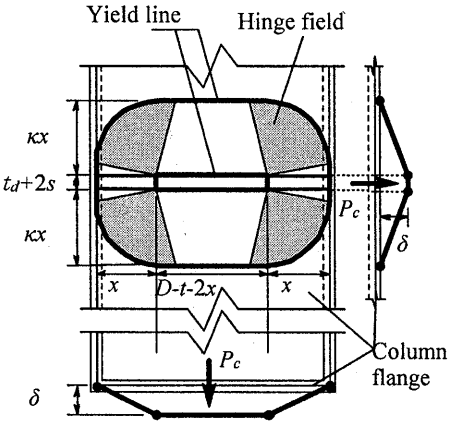

Fig.14 Out of plane collapse mechanism of column tubular wall for mechanism P_A

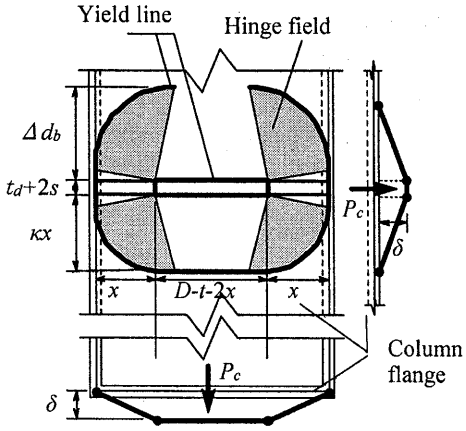

Fig.15 Out of plane collapse mechanism of column tubular wall for mechanism P_B

where, x : the plastic filed parameter of the column flange; t_d : exterior diaphragm thickness; a : the length of exterior diaphragm; b : the vertical distance from the corner of steel tube to the edge of beam flange; σ_{dy}: yield stress of diaphragm; δ : the virtual displacement of steel tube ($\delta = \Delta\theta \times \Delta d_b$).

For the mechanism P_A and P_B, the out-of-plane deformation of steel column flange is shown in Figs.14 and Fig.15. The internal virtual work of column flange (${}_sW_c^{P_A}$ and ${}_sW_c^{P_A}$) are given by Eqs.(8)[19] and (9).

$$ {}_sW_c^{P_A} = \left(\frac{t_d + 2s}{x} + \frac{D-t}{\kappa x} - \frac{2}{\kappa} + \frac{4}{\pi}(\log_e \kappa)^2 + \pi\right) t^2 \sigma_{cy} \delta \qquad (8) $$

$$ {}_sW_c^{P_B} = \left[\frac{D-t-2x}{4} + \frac{D-t-2x}{2\kappa x}\Delta d_b + \frac{t_d + 2s}{x}\Delta d_b + \frac{\Delta d_b}{\pi}\log_e \frac{\Delta d_b}{\pi} + \pi \Delta d_b \cdot \left\{1 + \frac{2}{\pi^2}(\log_e \kappa)^2 + \frac{2}{\pi^2}(\log_e \frac{\Delta d_b}{\pi})^2\right\}\right] t^2 \sigma_{cy} \delta \qquad (9) $$

where, s : the weld leg length; κ : the plastic filed parameter of the column flange; Δd_b : the difference in the beam depth.

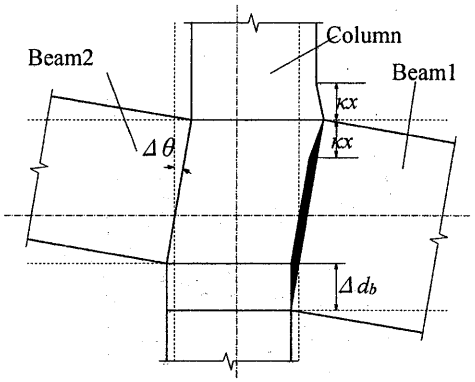

Fig.16 Collapse mechanism of beam1 web

For mechanism P_A, the beam1 web yields as shown in Fig.16. The internal virtual work of beam web (${}_sW_w$) is given by Eq. (10).

$$ {}_sW_w = 1/2\left(d_{b1} + d_{b2} - \kappa x\right) t_w \sigma_{wy} \Delta d_b \Delta\theta \qquad (10) $$

where, t_w : beam web thickness; σ_{wy} : yield stress of beam web.

The collapse mechanism of concrete panel is assumed as arch mechanism as shown in Fig.17. The internal virtual work of concrete (${}_cW_P^E$, ${}_cW_P^{P_A}$ and ${}_cW_P^{P_B}$) are given by Eqs. (11)[17], (12) and (13), respectively.

$$ {}_cW_P^E = \frac{{}_cD^2}{2}\left\{\sqrt{1 + \left(\frac{d_{b1}}{{}_cD}\right)^2} - \frac{d_{b1}}{{}_cD}\right\} {}_c\sigma_B d_{b1} \Delta\theta \qquad (11) $$

$$ {}_cW_P^{P_A} = \frac{{}_cD^2}{2}\left\{\sqrt{1 + \left(\frac{d_{b1}}{{}_cD}\right)^2} - \frac{d_{b1}}{{}_cD}\right\} {}_c\sigma_B d_{b1} \Delta\theta \qquad (12) $$

$$ {}_cW_P^{P_B} = \frac{{}_cD^2}{2}\left\{\sqrt{1 + \left(\frac{d_{b2}}{{}_cD}\right)^2} - \frac{d_{b2}}{{}_cD}\right\} {}_c\sigma_B d_{b2} \Delta\theta \qquad (13) $$

where, ${}_cD$: core concrete width, ${}_c\sigma_B$: concrete compressive strength.

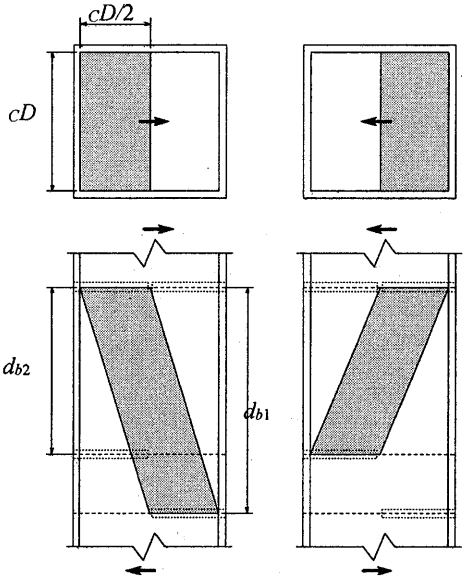

(a) Mechanism E, P_A (b) Mechanism P_B

Fig.17 Collapse mechanism of concrete panel

Based on the virtual work principle, the external virtual work equals to the internal virtual work. Thus,

$$ {}_pM_P^E \cdot \Delta\theta = {}_sW_P^E + {}_cW_P^E \qquad (14) $$

$$ {}_pM_p^{P_A I} \cdot \Delta\theta = {}_sW_P^{P_A} + {}_sW_c^{P_A} + W_d + {}_sW_w + {}_cW_p^{P_A} \qquad (15) $$

$$ {}_pM_p^{P_B I} \cdot \Delta\theta = {}_sW_P^{P_B} + {}_sW_c^{P_B} + W_d + {}_cW_p^{P_B} \qquad (16) $$

The plastic moment of mechanism P_A and P_B (${}_pM_p^{P_A}$, ${}_pM_p^{P_B}$) are given by the following equations.

$$ {}_pM_p^{P_A} = {}_pM_p^{P_A I} - ({}_cQ_U + {}_cQ_L)\Delta d_b / 2 \qquad (17) $$

$$ {}_pM_p^{P_B} = {}_pM_p^{P_B I} - ({}_cQ_U + {}_cQ_L)\Delta d_b / 2 \qquad (18) $$

Based on upper bound theory, the parameters of x and κ are given by partial derivative:

$$ \partial\, {}_pM_p^{P_A} / \partial x = 0 \,,\ \partial\, {}_pM_p^{P_A} / \partial\kappa = 0 \qquad (19), (20) $$

$$ \partial\, {}_pM_p^{P_B} / \partial x = 0 \,,\ \partial\, {}_pM_p^{P_B} / \partial\kappa = 0 \qquad (21), (22) $$

For the positive loading, the minimum plastic moment between ${}_pM_p^{P_A}$ and ${}_pM_P^E$ is selected as plastic moment of the connection panel. While for the negative loading, the minimum plastic moment between ${}_pM_p^{P_B}$ and ${}_pM_P^E$ is selected as plastic moment of the connection panel zone.

$$ {}_pM_p^+ = \min\{{}_pM_p^E, {}_pM_p^{P_A}\} \qquad (23) $$

$$ {}_pM_p^- = \min\{{}_pM_p^E, {}_pM_p^{P_B}\} \qquad (24) $$

The plastic shear strengths of entire panel under the positive and negative loadings (${}_pQ_p^+$, ${}_pQ_p^-$) are obtained by plastic moment and beam1 depth.

$$ {}_pQ_p^+ = {}_pM_p^+ / d_{b1} \quad (25) $$

$$ {}_pQ_p^- = {}_pM_p^+ / d_{b1} \quad (26) $$

The shear forces of entire panel obtained by calculation formulae are listed in Table4. Comparing the residual deformation of specimens with the assumed collapse mechanisms, the deformation of No.1 agrees with mechanism E, the failure model of No.2 and No.3 match well with the mechanism P_A under the positive loadings and the failure model of No.2 to No.4 agree with mechanism P_B under the negative loadings. Therefore, the calculated shear force of No.1 follows mechanism E. the calculated shear forces of No.2 and No.3 follow mechanism P_A under the positive loadings. While the calculated shear forces of No.2 to No.4 follow mechanism P_B under the negative loadings.

Table4 Calculated shear force of entire panel

No.	Δd_b [mm]	Positive loading		Negative loading	
		${}_pQ_E$ [kN]	${}_pQ_{PA}$ [kN]	${}_pQ_E$ [kN]	${}_pQ_{PB}$ [kN]
1	0	992	-	992	-
2	75	995	975	995	891
3	150	1,001	918	1,001	799
4	150	-	-	996	795

* ${}_pQ_E$, ${}_pQ_{PA}$ and ${}_pQ_{PB}$ represent the shear force of entire panel zone obtained by mechanism E, mechanism P_A and mechanism P_B, respectively.

Table5 Comparison between the strength calculation results and the experimental strength results

No	Δd_b (mm)	Positive loading			Negative loading			${}_pQ_{pg}$ (kN)
		${}_pQ_{pc}$ (kN)	${}_pQ_{pe}$ (kN)	${}_pQ_{pc}/{}_pQ_{pe}$	${}_pQ_{pc}$ (kN)	${}_pQ_{pe}$ (kN)	${}_pQ_{pc}/{}_pQ_{pe}$	
1	0	992	1,269	0.78	992	1,251	0.79	1,109
2	75	975	1,141	0.85	891	1,162	0.77	-
3	150	918	1,050	0.87	799	1,063	0.75	-
4		-	-	-	795	1,109	0.72	-

※${}_pQ_{pc}$: shear force of entire panel obtained by calculation; ${}_pQ_{pe}$: shear force of entire panel obtained by experimental results; ${}_pQ_{pg}$: shear force of entire panel obtained by Fukumoto formulae.

The comparisons between strength calculation results and the experimental strength results for the entire panel are listed in Table5. For the positive loading test, the calculation results underestimate the experimental results for 20%. While for the negative loading test, the calculation results underestimate the experimental results about 20%- 30%. The shear force of entire panel for No.1 obtained by Fukumoto formulae match well with the experimental results. One of the reason is that the Fukumoto formulae take the confinement provided by the steel tube flange into account.

4. Conclusive Remarks

In this paper, monotonic and cyclic performances of the offset H shaped steel beam to square concrete filled steel tube (CFT) column connections with exterior diaphragms are conducted. Certain conclusive remarks obtained by the test are summarized as follows:

(1) Assumed collapse mechanisms for both steel panel and concrete panel can predict the failure models of the specimens tested in the experiments.

(2) Offset H shaped steel beam to square CFT column connection panels with exterior diaphragms can form different collapse mechanisms under the different loading directions.

(3) Owing to the influence of difference in beam depth, the plastic strength of entire panel zone under the negative loading is a little higher than that under the positive loading.

(4) The proposed calculation formulae underestimate the experimental results about 20% to 30%.

Acknowledgements

This study was financially supported by Grant-in-Aid for Scientific Research (B) No. 25820268. Beside, members at Kawano lab from Kyusyu University are also gratefully acknowledged for significant supports on this study.

REFERENCES

1) Tabuchi, M., Kanatani, H. and Kamba, T.: On The Local Failure of RHS-Column to H-beam Connections: An experimental study on the welded RHS-column to beam connections Part 1, J. Struct. Constr., AIJ, Japan, No.349, pp. 71-80, March, 1985. (in Japanese)

2) Tabuchi, M., Kanatani, H. and Kamba, T.: Empirical Formulae For Local Strength of Welded RHS-Column to H-Beam Connections : An experimental study on the welded RHS-column to beam connections Part2. J. Struct. Constr., AIJ, Japan, No. 352, pp.79-89, June, 1985. (in Japanese)

3) Matsuo S., Tanaka T. and Inoue K.: Theoretical and experimental study on strength of RHS-column to beam connections with exterior diaphragm, J. Struct. Constr., AIJ, No.606, 225-232, August, 2006. (in Japanese)

4) Matsuo S., Tanaka T. and Inoue K.: Design formulae for RHS-column to beam connections with exterior diaphragms, J. Struct. Constr., AIJ, No.618, pp. 221-228, Aug., 2007 (in Japanese)

5) Kuwahara S., Kumamno T. and Inoue K.: The elasto-plastic behaviour of joint panels at the connection of rectangular steel column and two H-shaped beams with different depth, J. Struct. Constr., AIJ, No.533, pp. 175-181, July, 2000.

6) Matsuo S., Oyamada T., Ikeda R. and Tanaka T.: Elasto-plastic behavior of offset beam-to-column connection panels with exterior diaphragms, J. Struct. Constr., AIJ, Vol. 78, No.692, Oct., 2013. (in Japanese)
7) Matsui, C.: Local buckling of concrete filled steel square tubular columns, Proc., IABSE-ECCS Symp. on Steel in Building, IABSE,Rep. No. 48, 1985
8) Yokoyama, Y., Morita, K., Kawamata, Y., and Matsumura, H.: Structure behaviors of steel- beam to concrete-filled square tube column connections reinforced with inner ring stiffener, Proc., 3rd Int. Conf. on Steel-Concrete Composite Structures, Fukuoka, Japan, pp. 165-170. 1991.
9) Kawano, A., Matsui, C. and Murai, N.: Load-deformation Relationship Model for Local Deformations in Diaphragm-stiffened Connections of H-shaped Steel Beams to Rectangular CFT Column, Steel Construction Engineering, JSSC, Vol. 5, No. 17, pp. 93-104, 1998 (in Japanese).
10) Kanatami, H., Tabuchi, M., and Kamba, T.: A study on concrete filled RHS column to H-beam connections fabricated with HT bolts in rigid frames, proc., 1st Composite Construction in Steel and Concrete Conf., Engineering Foundation, New York，614-635, 1987.
11) Kawano, A., Matsui, C. and Murai, N.: A Test on the Connection Panel Behavior of H-shaped Beams to CFT Columns with High-Strength Concrete, Summaries of Technical Papers of Annual Meetings, Structures III, AIJ, Japan, pp. 1223-1224, 1999 (in Japanese).
12) Architectural Institute of Japan (AIJ). : AIJ standard for structural calculation of steel reinforced concrete structures. AIJ, Tokyo, Japan (1987)
13) Koester BD.: Panel zone behavior of moment connections between rectangular concrete-filled steel tubes and wide flange beams. [Ph.D. dissertation] Austin, Texas cbe: University of Texas; 2000.
14) Cheng CT, Chung LL.: Seismic performance of steel beams to concrete-filled steel tubular column connections. J Constr Steel Res;59(3):405-426, 2003
15) Cheng CT, Chan CF, Chung LL.: Seismic behavior of steel beams and CFT column moment-resisting connections with floor slabs. J Constr Steel Res; Vol. 63, No.11, pp. 1479-1149, 2007.
16) Fukumoto, T. and Morita, K.: Elasto-plastic Behavior of Steel beam to square CFT column Connections. Proceedings of the Sixth International Conference on Steel Concrete Composite Structures, Association for International Cooperation and Research in Steel Concrete Composite Structures (ASCCS), Los Angeles, USA, pp. 565-572. March 2000.
17) Fukumoto, T. and Taki, M.: Local Elastic-plastic Behavior of Steel Beam to Concrete Filled Square Steel Tube Column Connctions: External Diaphragm Connection Type Column to Wide Flange Beam Moment Connections. J. Struct. Constr., AIJ, Japan, No. 560, pp. 213-220, 2002. (in Japanese)
18) Kato, B., Akiyama, H and Yamanouchi, H.: Experimental law on the stress-strain history curve of steel（鋼材の応力ー ひずみ履歴曲線に関する実験則）, Summaries of Technical Papers of Annual Meeting AIJ, pp. 937-938, Oct., 1973. (in Japanese)
19) Mansfield E. H.: Studies in collapse analysis of rigid-plastic plates with a square yield diagram, Proc. Of the Royal Society London, 241, Series A, pp. 311-338, 1957.8.

（受理：平成26年5月29日）